

EUROPEAN ORGANIZATION FOR NUCLEAR RESEARCH

CERN-EP/2001-004

22-December-2000

Search for the Standard Model Higgs boson at LEP in the year 2000

DELPHI Collaboration

Abstract

Searches for the Standard Model Higgs boson have been performed in the data collected by the DELPHI experiment at LEP in the year 2000 at centre-of-mass energies between 200 and 209 GeV corresponding to a total integrated luminosity of 224 pb^{-1} . No evidence for a Higgs signal is observed in the kinematically accessible mass range, and a 95% CL lower mass limit of $114.3 \text{ GeV}/c^2$ is set, to be compared with an expected median limit of $113.5 \text{ GeV}/c^2$ for these data.

(Accepted by Phys.Lett.B)

arXiv:hep-ex/0102036v1 16 Feb 2001

P.Abreu²², W.Adam⁵¹, T.Adye³⁷, P.Adzic¹², Z.Albrecht¹⁹, T.Alderweireld², G.D.Alekseev¹⁸, R.Aleman⁹, T.Allmendinger¹⁹, P.P.Allport²³, S.Almehed²⁵, U.Amaldi²⁹, N.Amapane⁴⁶, S.Amato⁴⁸, E.Anashkin³⁶, E.G.Anassontzis³, P.Andersson⁴⁵, A.Andreazza²⁸, S.Andringa²², N.Anjos²², P.Antilogus²⁶, W-D.Apel¹⁹, Y.Arnoud¹⁶, B.Åsman⁴⁵, J-E.Augustin²⁴, A.Augustinus⁹, P.Baillon⁹, A.Ballestrero⁴⁶, P.Bambade^{9,21}, F.Barao²², G.Barbiellini⁴⁷, R.Barbier²⁶, D.Y.Bardin¹⁸, G.Barker¹⁹, A.Baroncelli³⁹, M.Battaglia¹⁷, M.Baubillier²⁴, K-H.Becks⁵³, M.Begalli⁶, A.Behrmann⁵³, Yu.Belokopytov⁹, K.Belous⁴³, N.C.Benekos³², A.C.Benvenuti⁵, C.Berat¹⁶, M.Berggren²⁴, L.Berntzon⁴⁵, D.Bertrand², M.Besancon⁴⁰, N.Besson⁴⁰, M.S.Bilenky¹⁸, D.Bloch¹⁰, H.M.Blom³¹, L.Bol¹⁹, M.Bonesini²⁹, M.Boonekamp⁴⁰, P.S.L.Booth²³, G.Borisov²¹, C.Bosio⁴², O.Botner⁴⁹, E.Boudinov³¹, B.Bouquet²¹, T.J.V.Bowcock²³, I.Boyko¹⁸, I.Bozovic¹², M.Bozzo¹⁵, M.Bracko⁴⁴, P.Branchini³⁹, R.A.Brenner⁴⁹, P.Bruckman⁹, J-M.Brunet⁸, L.Bugge³³, P.Buschmann⁵³, M.Caccia²⁸, M.Calvi²⁹, T.Camporesi⁹, V.Canale³⁸, F.Carena⁹, L.Carroll²³, C.Caso¹⁵, M.V.Castillo Gimenez⁵⁰, A.Cattai⁹, F.R.Cavallo⁵, M.Chapkin⁴³, Ph.Charpentier⁹, P.Checchia³⁶, G.A.Chelkov¹⁸, R.Chierici⁴⁶, P.Chliapnikov⁴³, P.Chochula⁷, V.Chorowicz²⁶, J.Chudoba³⁰, K.Cieslik²⁰, P.Collins⁹, R.Contri¹⁵, E.Cortina⁵⁰, G.Cosme²¹, F.Cossutti⁹, M.Costa⁵⁰, H.B.Crawley¹, D.Crennell³⁷, J.Croix¹⁰, G.Crosetti¹⁵, J.Cuevas Maestro³⁴, S.Czellar¹⁷, J.D'Hondt², J.Dalmau⁴⁵, M.Davenport⁹, W.Da Silva²⁴, G.Della Ricca⁴⁷, P.Delpierre²⁷, N.Demaria⁴⁶, A.De Angelis⁴⁷, W.De Boer¹⁹, C.De Clercq², B.De Lotto⁴⁷, A.De Min⁹, L.De Paula⁴⁸, H.Dijkstra⁹, L.Di Ciaccio³⁸, K.Doroba⁵², M.Dracos¹⁰, J.Drees⁵³, M.Dris³², G.Eigen⁴, T.Ekelof⁴⁹, M.Ellert⁴⁹, M.Elsing⁹, J-P.Engel¹⁰, M.Espirito Santo⁹, G.Fanourakis¹², D.Fassouliotis¹², M.Feindt¹⁹, J.Fernandez⁴¹, A.Ferrer⁵⁰, E.Ferrer-Ribas²¹, F.Ferro¹⁵, A.Firestone¹, U.Flagmeyer⁵³, H.Foeth⁹, E.Fokitis³², B.Franek³⁷, A.G.Frodesen⁴, R.Fruhvirth⁵¹, F.Fulda-Quenzer²¹, J.Fuster⁵⁰, D.Gamba⁴⁶, S.Gamblin²¹, M.Gandelman⁴⁸, C.Garcia⁵⁰, C.Gaspar⁹, M.Gaspar⁴⁸, U.Gasparini³⁶, Ph.Gavillet⁹, E.N.Gaziz³², D.Gele¹⁰, T.Geralis¹², N.Ghodbane²⁶, I.Gil⁵⁰, F.Glege⁵³, R.Gokieli^{9,52}, B.Golob^{9,44}, G.Gomez-Ceballos⁴¹, P.Goncalves²², I.Gonzalez Caballero⁴¹, G.Gopal³⁷, L.Gorn¹, Yu.Gouz⁴³, V.Gracco¹⁵, J.Grahl¹, E.Graziani³⁹, G.Grosdidier²¹, K.Grzelak⁵², J.Guy³⁷, C.Haag¹⁹, F.Hahn⁹, S.Hahn⁵³, S.Haider⁹, A.Hallgren⁴⁹, K.Hamacher⁵³, J.Hansen³³, F.J.Harris³⁵, S.Haug³³, F.Hauler¹⁹, V.Hedberg^{9,25}, S.Heising¹⁹, J.J.Hernandez⁵⁰, P.Herquet², H.Herr⁹, O.Hertz¹⁹, E.Higon⁵⁰, S-O.Holmgren⁴⁵, P.J.Holt³⁵, S.Hoorelbeke², M.Houlden²³, J.Hrubeč⁵¹, G.J.Hughes²³, K.Hultqvist^{9,45}, J.N.Jackson²³, R.Jacobsson⁹, P.Jalocha²⁰, Ch.Jarlskog²⁵, G.Jarlskog²⁵, P.Jarry⁴⁰, B.Jean-Marie²¹, D.Jeans³⁵, E.K.Johansson⁴⁵, P.Jonsson²⁶, C.Joram⁹, P.Juillot¹⁰, L.Jungermann¹⁹, F.Kapusta²⁴, K.Karafasoulis¹², S.Katsanevas²⁶, E.C.Katsoufis³², R.Keranen¹⁹, G.Kernel⁴⁴, B.P.Kersevan⁴⁴, B.A.Khomenko¹⁸, N.N.Khovanski¹⁸, A.Kiiskinen¹⁷, B.King²³, A.Kinvig²³, N.J.Kjaer⁹, O.Klapp⁵³, P.Kluit³¹, P.Kokkinias¹², V.Kostioukhine⁴³, C.Kourkoumelis³, O.Kouznetsov¹⁸, M.Krammer⁵¹, E.Kriznic⁴⁴, Z.Krumstein¹⁸, P.Kubinec⁷, M.Kucharczyk²⁰, J.Kurowska⁵², J.W.Lamsa¹, J-P.Laugier⁴⁰, G.Leder⁵¹, F.Ledroit¹⁶, L.Leinonen⁴⁵, A.Leisos¹², R.Leitner³⁰, G.Lenzen⁵³, V.Lepeltier²¹, T.Lesiak²⁰, M.Lethuillier²⁶, J.Libby³⁵, W.Liebig⁵³, D.Liko⁹, A.Lipniacka⁴⁵, I.Lippi³⁶, J.G.Loken³⁵, J.H.Lopes⁴⁸, J.M.Lopez⁴¹, R.Lopez-Fernandez¹⁶, D.Loukas¹², P.Lutz⁴⁰, L.Lyons³⁵, J.MacNaughton⁵¹, J.R.Mahon⁶, A.Maio²², A.Malek⁵³, S.Maltezos³², V.Malychev¹⁸, F.Mandl⁵¹, J.Marco⁴¹, R.Marco⁴¹, B.Marechal⁴⁸, M.Margoni³⁶, J-C.Marin⁹, C.Mariotti⁹, A.Markou¹², C.Martinez-Rivero⁹, S.Marti i Garcia⁹, J.Masik¹³, N.Mastroiannopoulos¹², F.Matorras⁴¹, C.Matteuzzi²⁹, G.Matthiae³⁸, F.Mazzucato^{36,14}, M.Mazzucato³⁶, M.Mc Cubbin²³, R.Mc Kay¹, R.Mc Nulty²³, E.Merle¹⁶, C.Meroni²⁸, W.T.Meyer¹, A.Miagkov⁴³, E.Migliore⁹, L.Mirabito²⁶, W.A.Mitaroff⁵¹, U.Mjoernmark²⁵, T.Moa⁴⁵, M.Moch¹⁹, K.Moenig^{9,11}, M.R.Monge¹⁵, J.Montenegro³¹, D.Moraes⁴⁸, P.Morettini¹⁵, G.Morton³⁵, U.Mueller⁵³, K.Muenich⁵³, M.Mulders³¹, L.M.Mundim⁶, W.J.Murray³⁷, B.Muryn²⁰, G.Myatt³⁵, T.Myklebust³³, M.Nassiakou¹², F.L.Navarría⁵, K.Nawrocki⁵², P.Negri²⁹, S.Nemeček¹³, N.Neufeld⁵¹, R.Nicolaidou⁴⁰, P.Niezurawski⁵², M.Nikolenko^{10,18}, V.Nomokonov¹⁷, A.Nygren²⁵, V.Obraztsov⁴³, A.G.Olshevski¹⁸, A.Onofre²², R.Orava¹⁷, K.Osterberg⁹, A.Ouraou⁴⁰, A.Oyanguren⁵⁰, M.Paganoni²⁹, S.Paiano⁵, R.Pain²⁴, R.Paiva²², J.Palacios³⁵, H.Palka²⁰, Th.D.Papadopoulou³², L.Pape⁹, C.Parkes²³, F.Parodi¹⁵, U.Parzefall²³, A.Passeri³⁹, O.Passon⁵³, L.Peralta²², V.Perepelitsa⁵⁰, M.Pernicka⁵¹, A.Perrotta⁵, C.Petridou⁴⁷, A.Petrolini¹⁵, H.T.Phillips³⁷, F.Pierre⁴⁰, M.Pimenta²², E.Piotto²⁸, T.Podobnik⁴⁴, V.Poireau⁴⁰, M.E.Pol⁶, G.Polok²⁰, P.Poropat⁴⁷, V.Pozdniakov¹⁸, P.Privitera³⁸, N.Pukhaeva¹⁸, A.Pullia²⁹, D.Radojicic³⁵, S.Ragazzi²⁹, H.Rahmani³², A.L.Read³³, P.Rebecchi⁹, N.G.Redaeli²⁹, M.Regler⁵¹, J.Rehn¹⁹, D.Reid³¹, R.Reinhardt⁵³, P.B.Renton³⁵, L.K.Resvanis³, F.Richard²¹, J.Ridky¹³, G.Rinaudo⁴⁶, I.Ripp-Baudot¹⁰, A.Romero⁴⁶, P.Ronchese³⁶, E.I.Rosenberg¹, P.Rosinsky⁷, P.Roudeau²¹, T.Rovelli⁵, V.Ruhlmann-Kleider⁴⁰, A.Ruiz⁴¹, H.Saarikko¹⁷, Y.Sacquin⁴⁰, A.Sadovsky¹⁸, G.Sajot¹⁶, L.Salmi¹⁷, J.Salt⁵⁰, D.Sampsonidis¹², M.Sannino¹⁵, A.Savoy-Navarro²⁴, C.Schwanda⁵¹, Ph.Schwemling²⁴, B.Schwering⁵³, U.Schwickerath¹⁹, F.Scuri⁴⁷, Y.Sedykh¹⁸, A.M.Segar³⁵, R.Sekulin³⁷, G.Sette¹⁵, R.C.Shellard⁶, M.Siebel⁵³, L.Simard⁴⁰, F.Simonetto³⁶, A.N.Sisakian¹⁸, G.Smadja²⁶, N.Smirnov⁴³, O.Smirnova²⁵, G.R.Smith³⁷, A.Sokolov⁴³, A.Sopczak¹⁹, R.Sosnowski⁵², T.Spaso⁹, E.Spiriti³⁹, S.Squarcia¹⁵, C.Stanescu³⁹, M.Stanitzki¹⁹, K.Stevenson³⁵, A.Stocchi²¹, J.Strauss⁵¹, R.Strub¹⁰, B.Stugu⁴, M.Szczekowski⁵², M.Szeptycka⁵², T.Tabarelli²⁹, A.Taffard²³, O.Tchikilev⁴³, F.Tegenfeldt⁴⁹, F.Terranova²⁹, J.Timmermans³¹, N.Tinti⁵, L.G.Tkatchev¹⁸, M.Tobin²³, S.Todorova⁹, B.Tome²², A.Tonazzo⁹, L.Tortora³⁹, P.Tortosa⁵⁰, D.Treille⁹, G.Tristram⁸, M.Trochimczuk⁵², C.Troncon²⁸, M-L.Turluer⁴⁰, I.A.Tyapkin¹⁸, P.Tyapkin²⁵, S.Tzamarias¹², O.Ullaland⁹, V.Uvarov⁴³, G.Valenti^{9,5}, E.Vallazza⁴⁷, C.Vander Velde², P.Van Dam³¹, W.Van den Boeck², W.K.Van Doninck², J.Van Eldik^{9,31}, A.Van Lysebetten², N.van Remortel², I.Van Vulpen³¹, G.Vegni²⁸, L.Ventura³⁶, W.Venus^{37,9}, F.Verbeure², P.Verdier²⁶, M.Verlato³⁶,

L.S.Vertogradov¹⁸, V.Verzi²⁸, D.Vilanova⁴⁰, L.Vitale⁴⁷, E.Vlasov⁴³, A.S.Vodopyanov¹⁸, G.Voulgaris³, V.Vrba¹³, H.Wahlen⁵³, A.J.Washbrook²³, C.Weiser⁹, D.Wicke⁹, J.H.Wickens², G.R.Wilkinson³⁵, M.Winter¹⁰, M.Witek²⁰, G.Wolf⁹, J.Yi¹, O.Yushchenko⁴³, A.Zalewska²⁰, P.Zalewski⁵², D.Zavrtanik⁴⁴, E.Zevgolatakos¹², N.I.Zimin^{18,25}, A.Zintchenko¹⁸, Ph.Zoller¹⁰, G.Zumerle³⁶, M.Zupan¹²

¹Department of Physics and Astronomy, Iowa State University, Ames IA 50011-3160, USA

²Physics Department, Univ. Instelling Antwerpen, Universiteitsplein 1, B-2610 Antwerpen, Belgium and IIHE, ULB-VUB, Pleinlaan 2, B-1050 Brussels, Belgium

and Faculté des Sciences, Univ. de l'Etat Mons, Av. Maistriau 19, B-7000 Mons, Belgium

³Physics Laboratory, University of Athens, Solonos Str. 104, GR-10680 Athens, Greece

⁴Department of Physics, University of Bergen, Allégaten 55, NO-5007 Bergen, Norway

⁵Dipartimento di Fisica, Università di Bologna and INFN, Via Irnerio 46, IT-40126 Bologna, Italy

⁶Centro Brasileiro de Pesquisas Físicas, rua Xavier Sigaud 150, BR-22290 Rio de Janeiro, Brazil and Depto. de Física, Pont. Univ. Católica, C.P. 38071 BR-22453 Rio de Janeiro, Brazil

and Inst. de Física, Univ. Estadual do Rio de Janeiro, rua São Francisco Xavier 524, Rio de Janeiro, Brazil

⁷Comenius University, Faculty of Mathematics and Physics, Mlynska Dolina, SK-84215 Bratislava, Slovakia

⁸Collège de France, Lab. de Physique Corpusculaire, IN2P3-CNRS, FR-75231 Paris Cedex 05, France

⁹CERN, CH-1211 Geneva 23, Switzerland

¹⁰Institut de Recherches Subatomiques, IN2P3 - CNRS/ULP - BP20, FR-67037 Strasbourg Cedex, France

¹¹Now at DESY-Zeuthen, Platanenallee 6, D-15735 Zeuthen, Germany

¹²Institute of Nuclear Physics, N.C.S.R. Demokritos, P.O. Box 60228, GR-15310 Athens, Greece

¹³FZU, Inst. of Phys. of the C.A.S. High Energy Physics Division, Na Slovance 2, CZ-180 40, Praha 8, Czech Republic

¹⁴Currently at DPNC, University of Geneva, Quai Ernest-Ansermet 24, CH-1211, Geneva, Switzerland

¹⁵Dipartimento di Fisica, Università di Genova and INFN, Via Dodecaneso 33, IT-16146 Genova, Italy

¹⁶Institut des Sciences Nucléaires, IN2P3-CNRS, Université de Grenoble 1, FR-38026 Grenoble Cedex, France

¹⁷Helsinki Institute of Physics, HIP, P.O. Box 9, FI-00014 Helsinki, Finland

¹⁸Joint Institute for Nuclear Research, Dubna, Head Post Office, P.O. Box 79, RU-101 000 Moscow, Russian Federation

¹⁹Institut für Experimentelle Kernphysik, Universität Karlsruhe, Postfach 6980, DE-76128 Karlsruhe, Germany

²⁰Institute of Nuclear Physics and University of Mining and Metallurgy, Ul. Kawiory 26a, PL-30055 Krakow, Poland

²¹Université de Paris-Sud, Lab. de l'Accélérateur Linéaire, IN2P3-CNRS, Bât. 200, FR-91405 Orsay Cedex, France

²²LIP, IST, FCUL - Av. Elias Garcia, 14-1º, PT-1000 Lisboa Codex, Portugal

²³Department of Physics, University of Liverpool, P.O. Box 147, Liverpool L69 3BX, UK

²⁴LPNHE, IN2P3-CNRS, Univ. Paris VI et VII, Tour 33 (RdC), 4 place Jussieu, FR-75252 Paris Cedex 05, France

²⁵Department of Physics, University of Lund, Sölvegatan 14, SE-223 63 Lund, Sweden

²⁶Université Claude Bernard de Lyon, IPNL, IN2P3-CNRS, FR-69622 Villeurbanne Cedex, France

²⁷Univ. d'Aix - Marseille II - CPP, IN2P3-CNRS, FR-13288 Marseille Cedex 09, France

²⁸Dipartimento di Fisica, Università di Milano and INFN-MILANO, Via Celoria 16, IT-20133 Milan, Italy

²⁹Dipartimento di Fisica, Univ. di Milano-Bicocca and INFN-MILANO, Piazza delle Scienze 2, IT-20126 Milan, Italy

³⁰IPNP of MFF, Charles Univ., Areal MFF, V Holesovickach 2, CZ-180 00, Praha 8, Czech Republic

³¹NIKHEF, Postbus 41882, NL-1009 DB Amsterdam, The Netherlands

³²National Technical University, Physics Department, Zografou Campus, GR-15773 Athens, Greece

³³Physics Department, University of Oslo, Blindern, NO-1000 Oslo 3, Norway

³⁴Dpto. Física, Univ. Oviedo, Avda. Calvo Sotelo s/n, ES-33007 Oviedo, Spain

³⁵Department of Physics, University of Oxford, Keble Road, Oxford OX1 3RH, UK

³⁶Dipartimento di Fisica, Università di Padova and INFN, Via Marzolo 8, IT-35131 Padua, Italy

³⁷Rutherford Appleton Laboratory, Chilton, Didcot OX11 0QX, UK

³⁸Dipartimento di Fisica, Università di Roma II and INFN, Tor Vergata, IT-00173 Rome, Italy

³⁹Dipartimento di Fisica, Università di Roma III and INFN, Via della Vasca Navale 84, IT-00146 Rome, Italy

⁴⁰DAPNIA/Service de Physique des Particules, CEA-Saclay, FR-91191 Gif-sur-Yvette Cedex, France

⁴¹Instituto de Física de Cantabria (CSIC-UC), Avda. los Castros s/n, ES-39006 Santander, Spain

⁴²Dipartimento di Fisica, Università degli Studi di Roma La Sapienza, Piazzale Aldo Moro 2, IT-00185 Rome, Italy

⁴³Inst. for High Energy Physics, Serpukov P.O. Box 35, Protvino, (Moscow Region), Russian Federation

⁴⁴J. Stefan Institute, Jamova 39, SI-1000 Ljubljana, Slovenia and Laboratory for Astroparticle Physics,

Nova Gorica Polytechnic, Kostanjevska 16a, SI-5000 Nova Gorica, Slovenia,

and Department of Physics, University of Ljubljana, SI-1000 Ljubljana, Slovenia

⁴⁵Fysikum, Stockholm University, Box 6730, SE-113 85 Stockholm, Sweden

⁴⁶Dipartimento di Fisica Sperimentale, Università di Torino and INFN, Via P. Giuria 1, IT-10125 Turin, Italy

⁴⁷Dipartimento di Fisica, Università di Trieste and INFN, Via A. Valerio 2, IT-34127 Trieste, Italy

and Istituto di Fisica, Università di Udine, IT-33100 Udine, Italy

⁴⁸Univ. Federal do Rio de Janeiro, C.P. 68528 Cidade Univ., Ilha do Fundão BR-21945-970 Rio de Janeiro, Brazil

⁴⁹Department of Radiation Sciences, University of Uppsala, P.O. Box 535, SE-751 21 Uppsala, Sweden

⁵⁰IFIC, Valencia-CSIC, and D.F.A.M.N., U. de Valencia, Avda. Dr. Moliner 50, ES-46100 Burjassot (Valencia), Spain

⁵¹Institut für Hochenergiephysik, Österr. Akad. d. Wissensch., Nikolsdorfergasse 18, AT-1050 Vienna, Austria

⁵²Inst. Nuclear Studies and University of Warsaw, Ul. Hoza 69, PL-00681 Warsaw, Poland

⁵³Fachbereich Physik, University of Wuppertal, Postfach 100 127, DE-42097 Wuppertal, Germany

1 Introduction

The LEP accelerator was successfully operated at e^+e^- collision energies up to 209 GeV during the year 2000. The DELPHI experiment has collected more than 224 pb^{-1} at centre-of-mass energies above 200 GeV, extending the range of searches for the Standard Model Higgs boson above the previous limits obtained by DELPHI [1,2,3], by the other LEP collaborations, and by their combination by the LEP Higgs Working Group [4].

The results shown in this letter are based on the detector calibration obtained shortly after the end of data taking. They will be included in the preliminary combination of the LEP collaborations results on the 2000 year data [5], being prepared by the LEP Higgs Working group [6].

1.1 Data and simulation samples

The data used in this analysis, corresponding to a total of 224.1 pb^{-1} collected by the DELPHI detector in 2000, were analysed in the following subsamples: 2.3 pb^{-1} at an average centre-of-mass energy of 202.6 GeV, 6.7 pb^{-1} at 203.9 GeV, 10.5 pb^{-1} at 204.8 GeV, 62.5 pb^{-1} at 205.2 GeV, 18.2 pb^{-1} at 206.2 GeV, 115.2 pb^{-1} at 206.7 GeV and 8.7 pb^{-1} at 208.2 GeV.

Monte Carlo samples for background events were produced at fixed centre-of-mass energies of 202, 204, 205, 206, 207 and 208 GeV using the same simulation setup as for the 1999 analysis [1]. The samples correspond to about 200 times the collected luminosity.

Similarly, signal events were produced using the HZHA [7] generator, varying the Higgs boson mass from $85 \text{ GeV}/c^2$ to $120 \text{ GeV}/c^2$ in $5 \text{ GeV}/c^2$ steps, plus a fine scan in the most interesting zone, with samples simulated for mass hypotheses 108, 110, 112, 114 and $115 \text{ GeV}/c^2$.

1.2 Detector overview

A detailed description of the DELPHI apparatus can be found in [8]. For the first three quarters of the year the detector was operated in nominal conditions.

Data collected after the 1st of September, corresponding to the last 60 pb^{-1} , were affected by the complete failure of one sector (S6) of the TPC detector, which amounts to 1/12 of the TPC acceptance. Charged particle tracks crossing this sector were reconstructed using the information from the Vertex, Inner and Outer detectors, so the effect on the efficiency is limited. A complete sample of background and signal channels simulated with this TPC sector off was used to incorporate the small effect on the reconstructed event kinematics and the impact on the b-tagging efficiency into the analysis of this data sample.

To follow more precisely the change of conditions during the data taking, the calibration of the impact parameter resolution was performed with the high energy four-jet events. The same procedure was applied to the simulation where the four-jet events were selected with the same criteria and appropriately weighted according to the predicted cross-sections of the corresponding processes.

The calibration of the b-tagging used the tracks with negative impact parameter, while only the tracks with positive impact parameter were used in the lifetime based b-tagging.

The number of tracks with negative impact parameter is not affected by the calibration, and is used as further information in the b-tagging. Therefore this calibration

procedure is not correlated with the physics measurement, while it improves significantly the agreement between data and simulation.

The overall performance of the combined b-tagging in hadronic radiative return events ($e^+e^- \rightarrow Z^0 \gamma$), collected during the year 2000, is illustrated in Fig. 1. Effects of possible imperfect modelling of the high b-tag tail from non-b quarks were checked using the high energy semileptonic W^+W^- data and are also shown in Fig. 1.

2 Standard Model Higgs search

The previous LEP combined limit[4] on the Higgs mass at 95% CL was close to $108 \text{ GeV}/c^2$. Given the integrated luminosity corresponding to the data taken in the year 2000, the analysis is expected to cover efficiently the mass range up to the kinematical limit allowed by the increase in centre-of-mass energy.

The following improvements for this high mass range have been introduced in the analysis of the two main channels.

The four-jet analysis benefits from a better tuned b-tagging procedure and although it keeps the same event variables in the analysis, the discriminant neural network has been optimized for the high mass hypotheses.

The missing-energy channel includes a tighter preselection and additional variables in the likelihood, resulting in a better background rejection for a high mass Higgs; it is described in the following section.

2.1 $H\nu\bar{\nu}$ channel

In this channel both the preselection and the final discriminating likelihood have been reoptimised in the spirit of a “background free” analysis. A set of stringent cuts [9] was applied prior to the construction of the likelihood.

The discriminating likelihood includes six variables defined after forcing the event into a two-jet configuration with the DURHAM [10] algorithm: acoplanarity, acollinearity, polar angle of the missing momentum with respect to the beam direction, b-tagging, invariant mass in the transverse plane, the minimum of the energies around the most isolated particle and around the most energetic particle (normalised to their own energy). Three more variables are defined leaving the number of jets free in the DURHAM algorithm with $y_{cut} = 0.005$: the minimum angle between the jet directions and the missing momentum in the transverse plane, the minimal jet charged multiplicity, and the maximum track or reconstructed lepton transverse momentum with respect to the jet axis.

The effect of the preselection on data and simulated samples is shown in Table 1. After a tighter cut to select the most significant candidates, three candidate events remain, while 4.9 are expected according to the background simulation.

Distributions for the most relevant variables in this analysis are shown both at preselection level (Fig. 2), and at the tight selection level (Fig. 3).

The reconstructed Higgs boson mass is defined as the visible mass given by a one-constraint fit where the recoil system is assumed to be an on-shell Z^0 boson. It is used, together with the discriminant likelihood, in the two-dimensional computation of the confidence levels for the Higgs hypotheses.

Selection	Data	Background	$q\bar{q}(\gamma)$	4-fermion	Efficiency
H $\nu\bar{\nu}$ channel					
preselection	970	880	467	390	67%
candidates selection	90	99.7	50.4	49.3	60%
tight selection	3	4.9	1.4	3.5	30%
He $^+e^-$ channel					
preselection	1242	1172	745	416	78%
candidates selection	7	11.6	0.5	10.4	57%
tight selection	1	3.5	0.1	3.2	49%
H $\mu^+\mu^-$ channel					
preselection	3780	3763	2671	1067	81%
candidates selection	7	10.6	0.2	10.4	67%
tight selection	2	3.6	0.1	3.5	56%
$\tau^+\tau^-q\bar{q}$ channel					
preselection	9180	8913	5425	3468	98%
candidates selection	5	6.0	0.4	5.6	22%
tight selection	2	4.1	0.1	4.0	19%
H $q\bar{q}$ channel					
preselection	2266	2342	680	1662	85%
candidates selection	398	423.7	154.9	268.8	79%
tight selection	8	7.4	2.8	4.6	36%

Table 1: Effect of the selection cuts on data, simulated background and simulated signal events. The two main background contributions are detailed. Efficiencies are given for a signal of $m_H = 114 \text{ GeV}/c^2$. Candidates selection indicates the number of events used as input to the confidence level calculations. The tight selection is obtained after a further cut in the corresponding discriminant variable, and corresponds to the one used in the mass plot (Fig. 7).

2.2 Leptonic channels

Higgs boson searches in events with jets and leptons follow the analysis applied to the 1999 data [1], which included a \sqrt{s} dependence in the corresponding preselections. The effect of the selections on data and simulated samples is detailed in Table 1. Good agreement between data and background simulation at the preselection level is observed in all the leptonic channels.

In the He $^+e^-$ channel, 7 candidate events are selected in the data, for a total expected background of 11.6 events coming mainly from the $e^+e^-q\bar{q}$ process. In the H $\mu^+\mu^-$ channel, 7 events are selected and 10.6 background events are expected coming mainly from the $\mu^+\mu^-q\bar{q}$ process. Both channels use the b-tagging value as the discriminant variable and the fitted hadronic mass in the two-dimensional calculation of the confidence levels. One of the He $^+e^-$ and two of the H $\mu^+\mu^-$ candidates have a significant b-tagging value but are kinematically compatible with the ZZ hypothesis.

In the $\tau^+\tau^-q\bar{q}$ channel, 5 candidates are selected, while 6.0 are expected from the Standard Model background, which is dominated by the ZZ into $\tau^+\tau^-q\bar{q}$ process. Two

events are selected after a cut on the discriminant likelihood at 0.1; neither has a high value for the rescaled mass.

2.3 Higgs boson searches in four-jet events

Higgs boson searches in fully hadronic final states start with a common four-jet pre-selection [2,3], which eliminates hard radiative events and reduces the $q\bar{q}(\gamma)$ and $Z\gamma^*$ background, forcing all selected events into a four-jet topology with the DURHAM algorithm.

The performance of the DELPHI b-tagging procedure in the four-jet analysis was specially optimized and enhanced by taking into account the dependence on additional variables related to the kinematical properties of b-hadrons produced in decays of the Higgs boson. These variables, defined for each jet in the event, are: the polar angle of the jet direction, the jet energy, the charged multiplicity of the jet, the angle to the nearest jet, the average transverse momentum of charged particles with respect to the jet direction, the number of particles with negative impact parameter and the invariant mass of the jet. Including this dependence in the tagging algorithm significantly improves the rejection of the light quark background. The global b-tagging value of the event is defined as the maximum b-tagging value for any di-jet in the event, computed as the sum of the corresponding jet b-tagging values.

The final discriminant variable used in the four-jet channel is defined as the output of an artificial neural network (ANN) which combines 13 variables.

The first variable is the global b-tagging value of the event.

The next four variables rely on kinematics and test the compatibility of the event with the hypotheses of W^+W^- and ZZ production to either 4 or 5 jets. Constrained fits are used to derive the probability density function measuring the compatibility of the event kinematics with the production of two objects of any masses. This two-dimensional probability, the ideogram probability [11], is then folded with the expected mass distributions for the W^+W^- and ZZ processes, respectively.

Finally, the last eight input variables intended to reduce the $q\bar{q}(\gamma)$ contamination are the sum of the second and fourth Fox-Wolfram moments, the product of the minimum jet energy and the minimum opening angle between any two jets, the maximum and minimum jet momenta, the sum of the multiplicities of the two jets with lowest multiplicity, the sum of the masses of the two jets with lowest masses, the minimum di-jet mass and the minimum sum of the cosines of the opening angles of the two di-jets when considering all possible pairings of the jets. In the previous analysis [1] these eight variables were separately combined in an anti-QCD artificial neural network.

Fig. 4 shows the performance of the final discriminating variable in the efficiency-background plane for a $114 \text{ GeV}/c^2$ signal at $\sqrt{s} = 206.7 \text{ GeV}$.

The choice of the Higgs di-jet makes use of both the kinematical 5C-fit probabilities and the b-tagging information in the event [3]. The likelihood pairing function,

$$\mathcal{P}_b^{j_1} \cdot \mathcal{P}_b^{j_2} \cdot ((1 - R_b^Z - R_c^Z) \cdot \mathcal{P}_q^{j_3} \cdot \mathcal{P}_q^{j_4} + R_b^Z \cdot \mathcal{P}_b^{j_3} \cdot \mathcal{P}_b^{j_4} + R_c^Z \cdot \mathcal{P}_c^{j_3} \cdot \mathcal{P}_c^{j_4}) \cdot P_{j_3, j_4}^{5C}$$

is calculated for each of the six possibilities to combine the jets j_1, j_2, j_3 and j_4 . $\mathcal{P}_b^{j_i}, \mathcal{P}_c^{j_i}, \mathcal{P}_q^{j_i}$ are the probability densities of getting the observed b-tagging value for the jet j_i when originating from a b, c or light quark, estimated from simulation. R_b^Z and R_c^Z are the hadronic branching fractions of the Z^0 into b or c quarks, and P_{j_3, j_4}^{5C} is the probability corresponding to the kinematical 5C-fit with the jets j_3 and j_4 assigned to the Z^0 . The pairing that maximises this function is selected. The proportion of right matchings for the Higgs di-jet, estimated in simulated signal events with $114 \text{ GeV}/c^2$

mass, is around 53% at preselection level, increasing to above 70% at the tighter level, keeping a low rate of wrong pairings for ZZ background events.

The good agreement between data and background simulation after the four-jet preselection is illustrated in Fig. 5 which shows the distributions of the global b-tagging, the two ideogram probabilities for the configuration with 4 jets, and the output of the anti-QCD ANN. The results for the different selection levels are given in Table 1. The tighter cut at an ANN value of 0.7 selects 8 events in data while 7.4 are expected from the background simulation. Fig. 6 shows the previous variables at this level.

2.4 Confidence level estimation

The confidence levels for the background (CL_b) and signal plus background (CL_{s+b}) hypotheses are defined as the probability in the two cases of observing a likelihood ratio \mathcal{Q} , greater than or equal to that measured in the data [12]. The confidence level for the signal case is calculated consistently with the LEP Higgs Working group using the conservative ratio $CL_s = CL_{s+b}/CL_b$.

The likelihood ratio for a given Higgs mass hypothesis is defined as $\ln(\mathcal{Q}) = -S + \sum_i \ln(1 + s_i/b_i)$ where S is the total expected signal, and s_i and b_i are the signal and background probability densities for each candidate i , calculated using two-dimensional information, where one dimension is the reconstructed Higgs boson mass and the other is the channel dependent discriminant variable.

These densities are represented as two-dimensional histograms which are derived from the simulation samples described in section 1.1. These distributions are then smoothed using a two-dimensional kernel, which is essentially Gaussian but with a small longer tailed component. The width of the kernel varies from point to point, such that the statistical uncertainty on the estimated background is never more than 30%. The same width is applied to background and all signal samples to eliminate the possibility of the smearing itself increasing the estimated signal to background ratio. Finally the distribution is reweighted so that when projected onto either axis it has the same distribution as would have been observed if the smoothing had been only in one dimension. This makes better use of the simulation statistics if there are features which are essentially one dimensional, such as mass peaks, and it has been verified that the systematic errors introduced are significantly smaller than the statistical ones.

The resultant two-dimensional distributions are then linearly interpolated from the simulation conditions to the appropriate beam energy and Higgs mass hypotheses.

3 Results

The distribution of the reconstructed Higgs boson mass summed over all channels, at the level of the tight selection, is presented in Fig. 7.

The limit on the Standard Model Higgs boson mass is set combining the data analysed in the previous sections with those taken at lower energies, namely 161 and 172 GeV [13], 183 GeV [3], 189 GeV [2] and 192-202 GeV [1].

The confidence level for the signal hypothesis CL_s is shown in Fig. 8, as well as the confidence level for the background hypothesis in the form $1-CL_b$. A slight deficit with respect to the expected background is observed, and a 95% CL lower limit on the mass is set at 114.3 GeV/ c^2 while the expected median is 113.5 GeV/ c^2 . The test-statistic (negative log-likelihood ratio) is shown in Fig. 9.

It has been noticed that the combined LEP result [6] is better described if a Higgs boson with mass $115 \text{ GeV}/c^2$ is present. For such a signal, the DELPHI CL_{s+b} value is 3%, while the CL_b is 23%. The CL_s for this hypothesis is 12%, so that the present data are not incompatible with the existence of a Higgs boson with this mass. This can also be seen in Fig. 9, where the result is compared with the probability density for background and background plus signal experiments.

4 Conclusions

The data taken by DELPHI at 200-209 GeV in the year 2000 have been analysed to search for the Standard Model Higgs boson. The data for all channels is compatible with expectations from the Standard Model background. In combination with previous DELPHI results at lower centre-of-mass energies, a lower limit at 95% CL on the mass of the Standard Model Higgs boson is set at $114.3 \text{ GeV}/c^2$, while the expected median limit is $113.5 \text{ GeV}/c^2$.

Acknowledgements

We are extremely grateful to the members of CERN-SL Division for their expertise and dedication that has allowed the LEP energy to be increased well beyond the design value, with a consequent extension of the search for the Higgs boson. We are greatly indebted to our technical collaborators and to the funding agencies for their support in building and operating the DELPHI detector.

We acknowledge in particular the support of

Austrian Federal Ministry of Science and Traffics, GZ 616.364/2-III/2a/98,

FNRS-FWO, Flanders Institute to encourage scientific and technological research in the industry (IWT), Belgium,

FINEP, CNPq, CAPES, FUJB and FAPERJ, Brazil,

Czech Ministry of Industry and Trade, GA CR 202/96/0450 and GA AVCR A1010521,

Commission of the European Communities (DG XII),

Direction des Sciences de la Matière, CEA, France,

Bundesministerium für Bildung, Wissenschaft, Forschung und Technologie, Germany,

General Secretariat for Research and Technology, Greece,

National Science Foundation (NWO) and Foundation for Research on Matter (FOM),

The Netherlands,

Norwegian Research Council,

State Committee for Scientific Research, Poland, 2P03B06015, 2P03B11116 and SPUB/P03/DZ3/99,

JNICT-Junta Nacional de Investigação Científica e Tecnológica, Portugal,

Vedecka grantova agentura MS SR, Slovakia, Nr. 95/5195/134,

Ministry of Science and Technology of the Republic of Slovenia,

CICYT, Spain, AEN99-0950, AEN99-0761

The Swedish Natural Science Research Council,

Particle Physics and Astronomy Research Council, UK,

Department of Energy, USA, DE-FG02-94ER40817,

References

- [1] DELPHI Collab., DELPHI 2000-092 CONF 391, contributed paper for ICHEP2000, Osaka (abstract # 619).
- [2] DELPHI Collab., P. Abreu et al., Eur. Phys. J. **C17** (2000) 187.
- [3] DELPHI Collab., P. Abreu et al., Eur. Phys. J. **C10** (1999) 563.
- [4] ALEPH, DELPHI, L3 and OPAL Collab., The LEP working group for Higgs boson searches, CERN-EP/2000-055.
- [5] ALEPH Collaboration, Phys. Lett. **B495** (2000) 1
L3 Collaboration, Phys. Lett. **B495** (2000) 18
OPAL Collaboration *Search for the Standard Model Higgs Boson in e^+e^- collisions at $\sqrt{s} = 192\text{-}209$ GeV*, in preparation, to be submitted to Phys. Lett. B.
- [6] ALEPH, DELPHI, L3 and OPAL Collab., The LEP working group for Higgs boson searches, *Searches for the Standard Model Higgs Boson at LEP*, in preparation, to be submitted to Phys. Lett. B.
- [7] P. Janot, in CERN Report 96-01, Vol. 2, p. 309 (1996).
- [8] DELPHI Collab., P. Aarnio et al., Nucl. Instr. Meth. **A303** (1991) 233.
DELPHI Collab., P. Abreu et al., Nucl. Instr. Meth. **A378** (1996) 57.
DELPHI Silicon Tracker Group, P. Chochula et al., Nucl. Instr. Meth. **A412** (1998) 304.
- [9] DELPHI Collab., DELPHI 2000-077 CONF 376, contributed paper for ICHEP2000, Osaka (abstract # 275).
- [10] S. Catani, Yu.L.Dokshitzer, M.Olsson, G.Turnock and B.R.Webber, Phys.Lett.**B269** (1991) 432.
- [11] DELPHI Collab., P. Abreu et al., Phys. Lett **B462** (1999) 410.
- [12] A.L. Read, in CERN Report 2000-005, p. 81 (2000).
- [13] DELPHI Collab., P. Abreu et al., Eur. Phys. J. **C2** (1998) 1.

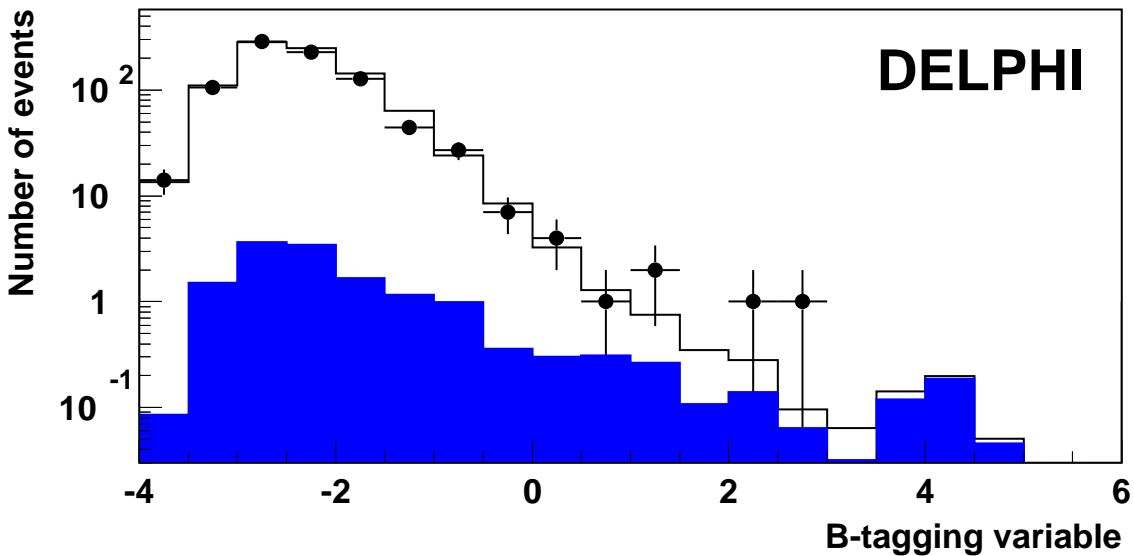
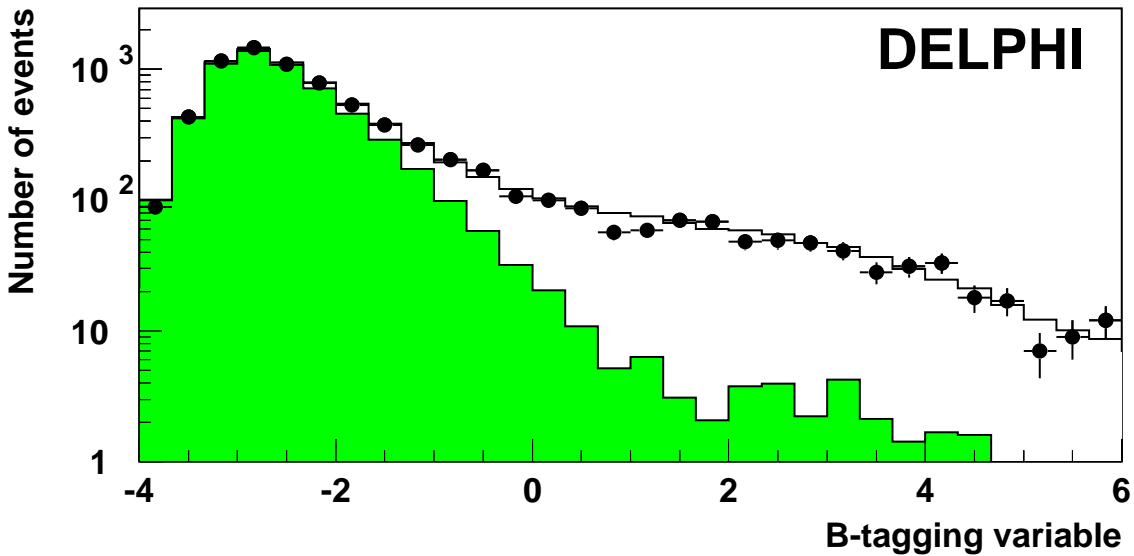


Figure 1: Top: distributions of the combined b-tagging variable, for the year 2000 radiative return $Z\gamma$ data (dots) and simulation (histogram). The expected contribution of $udsc$ -quarks and non- $q\bar{q}\gamma$ background is shown as the dark histogram. Bottom: same distribution for semileptonic W^+W^- high energy events in the 2000 data. The shaded histogram corresponds to the expected contribution from other processes, and shows the high purity of the selection.

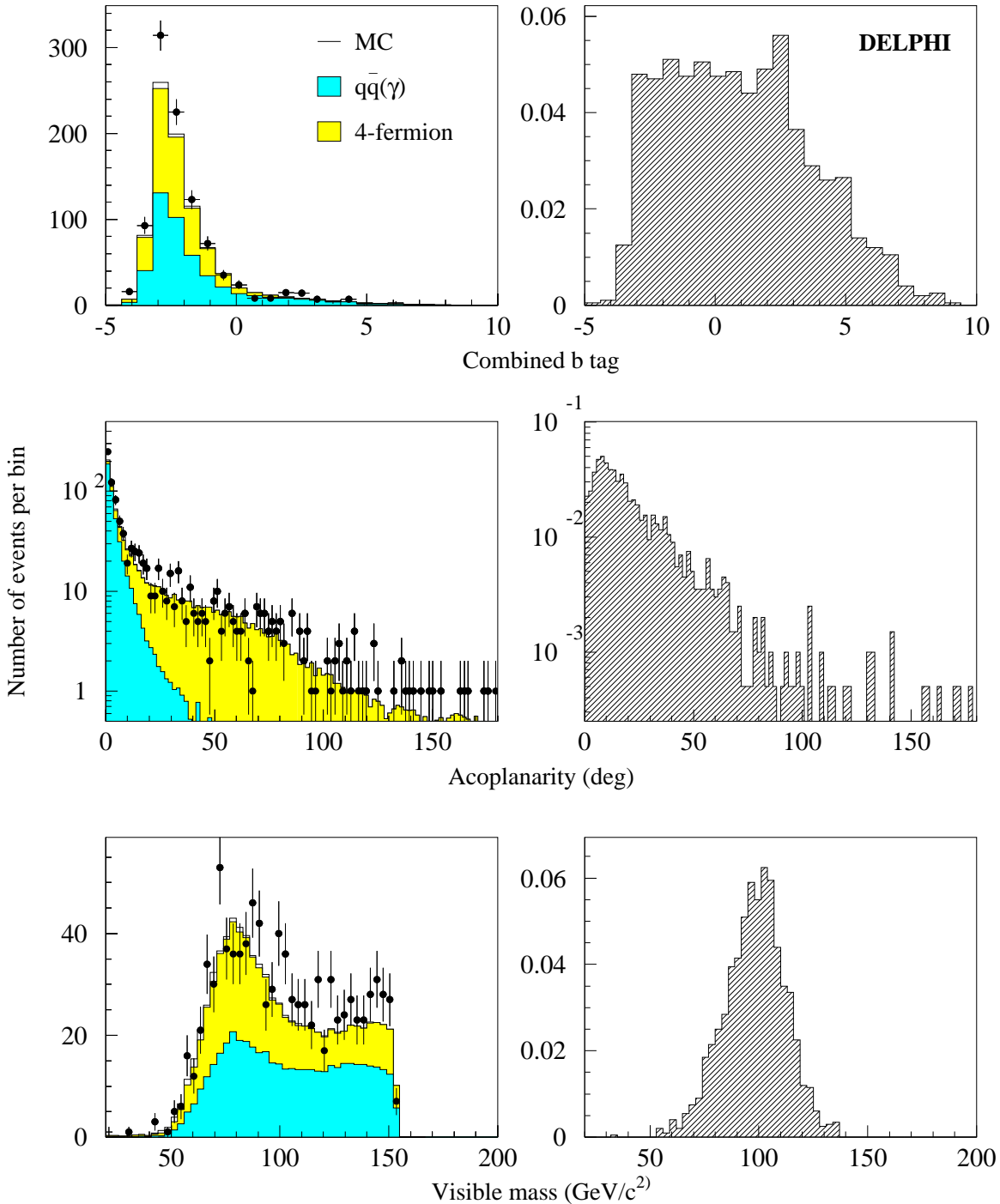


Figure 2: $H\nu\bar{\nu}$ channel: distributions of relevant analysis variables, at the preselection level. Data at $\sqrt{s} = 200\text{-}209 \text{ GeV}$ (dots) are compared with Standard Model background expectations (left-hand side histograms) and with the expected distribution for a $114 \text{ GeV}/c^2$ Higgs mass signal (right-hand side histogram).

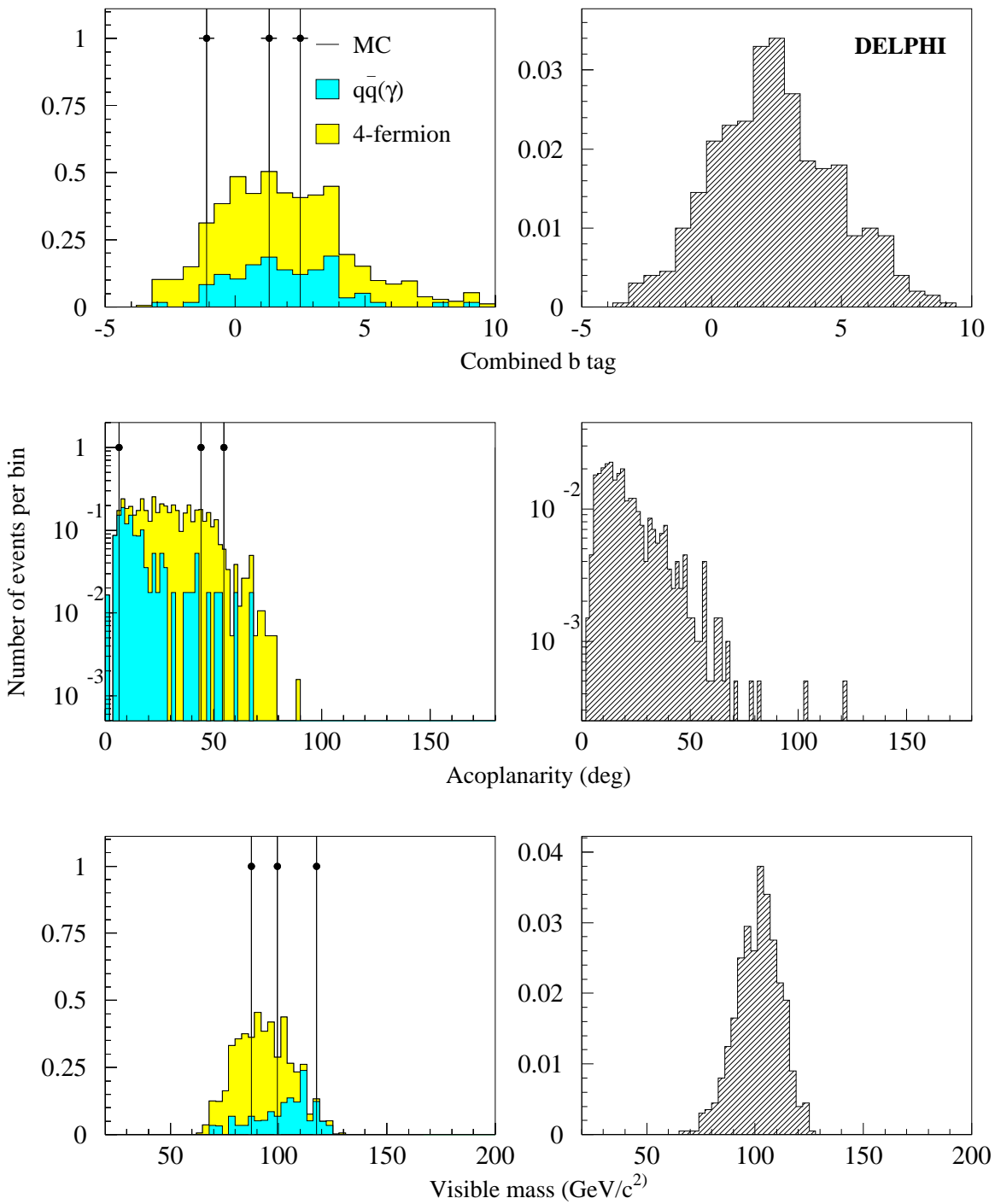


Figure 3: $H\nu\bar{\nu}$ channel: same distributions as in Fig.2 but at the tight selection level.

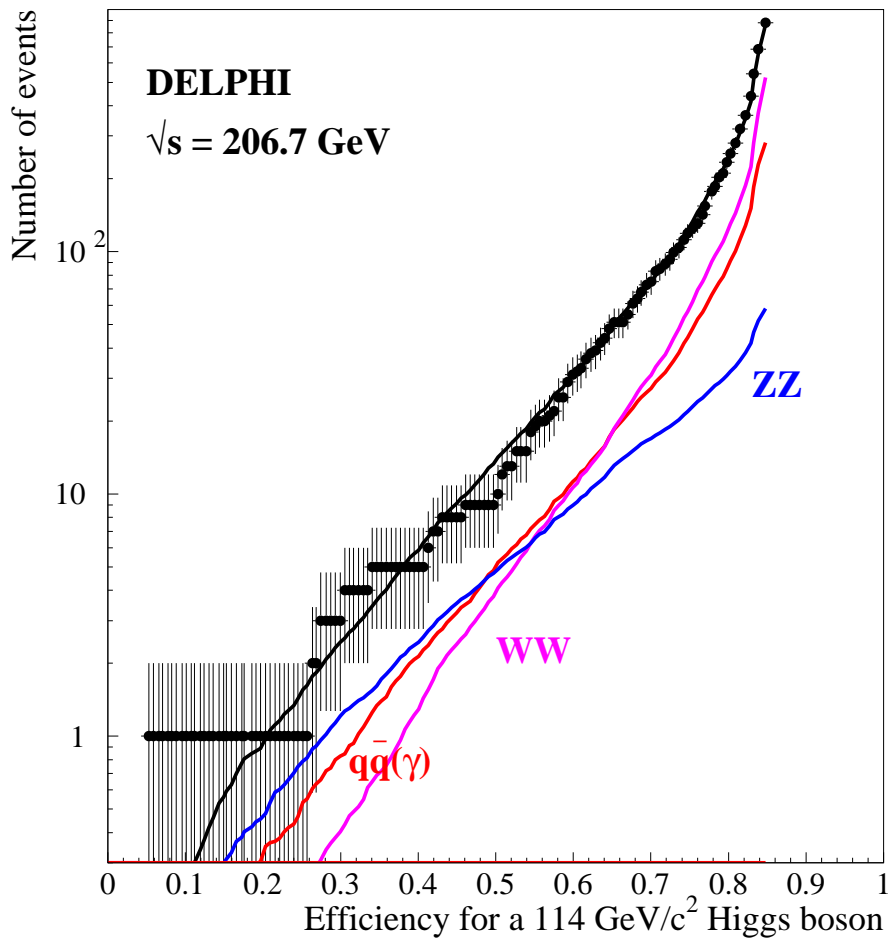


Figure 4: $Hq\bar{q}$ channel: Expected Standard Model background rate at a centre-of-mass energy $\sqrt{s} = 206.7 \text{ GeV}$ as a function of the efficiency for a $114 \text{ GeV}/c^2$ Higgs mass signal when varying the cut on the neural network variable. The different background contributions are shown summed and separately. Dots stand for data.

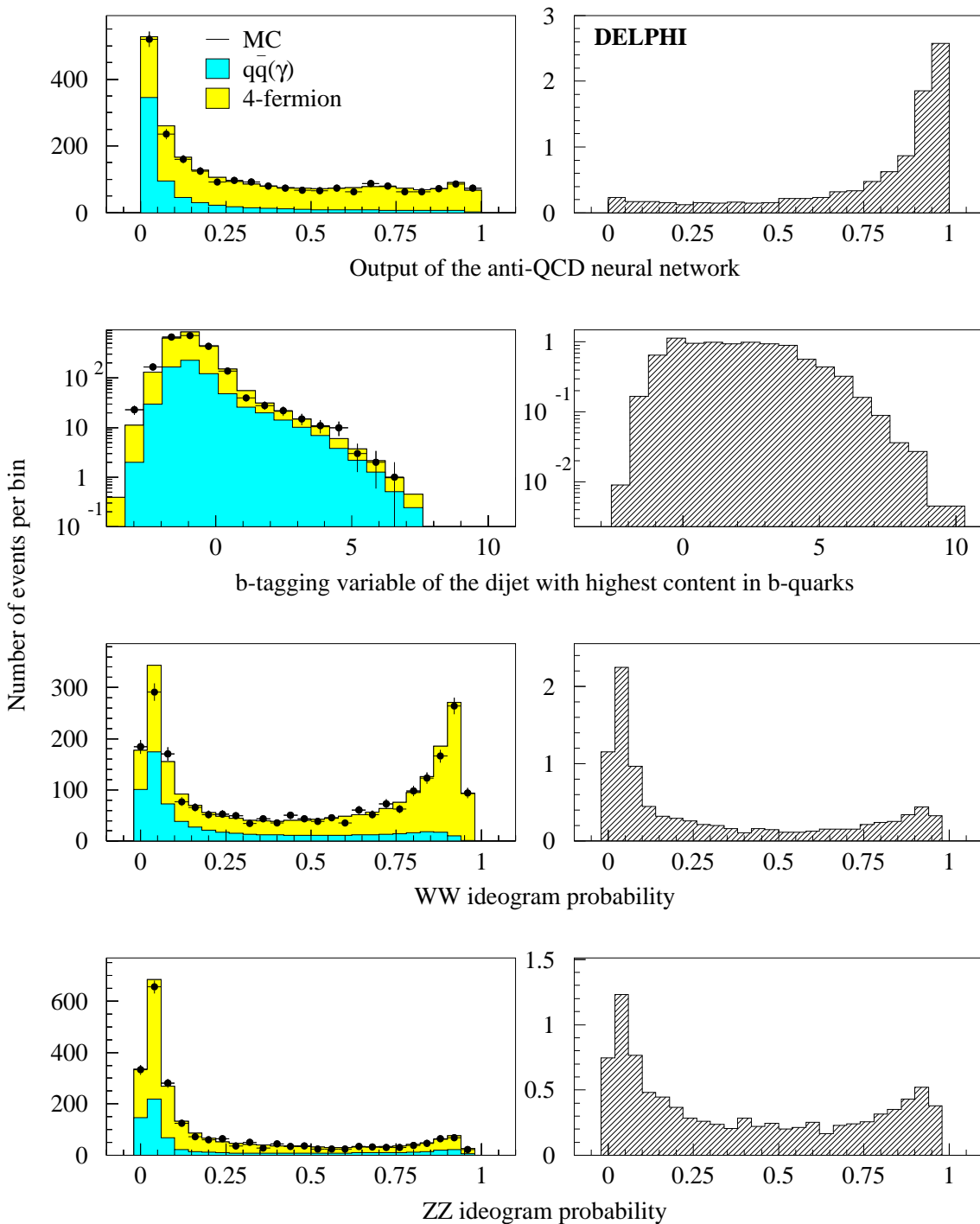


Figure 5: $Hq\bar{q}$ channel: distributions of relevant analysis variables at the preselection level. The eight variables used to reduce the $q\bar{q}(\gamma)$ background are summarized by the output of the anti-QCD neural network. Data at $\sqrt{s} = 200\text{-}209 \text{ GeV}$ (dots) are compared with Standard Model background expectations (left-hand side histograms) and with the expected distribution for a $114 \text{ GeV}/c^2$ Higgs mass signal (right-hand side histogram).

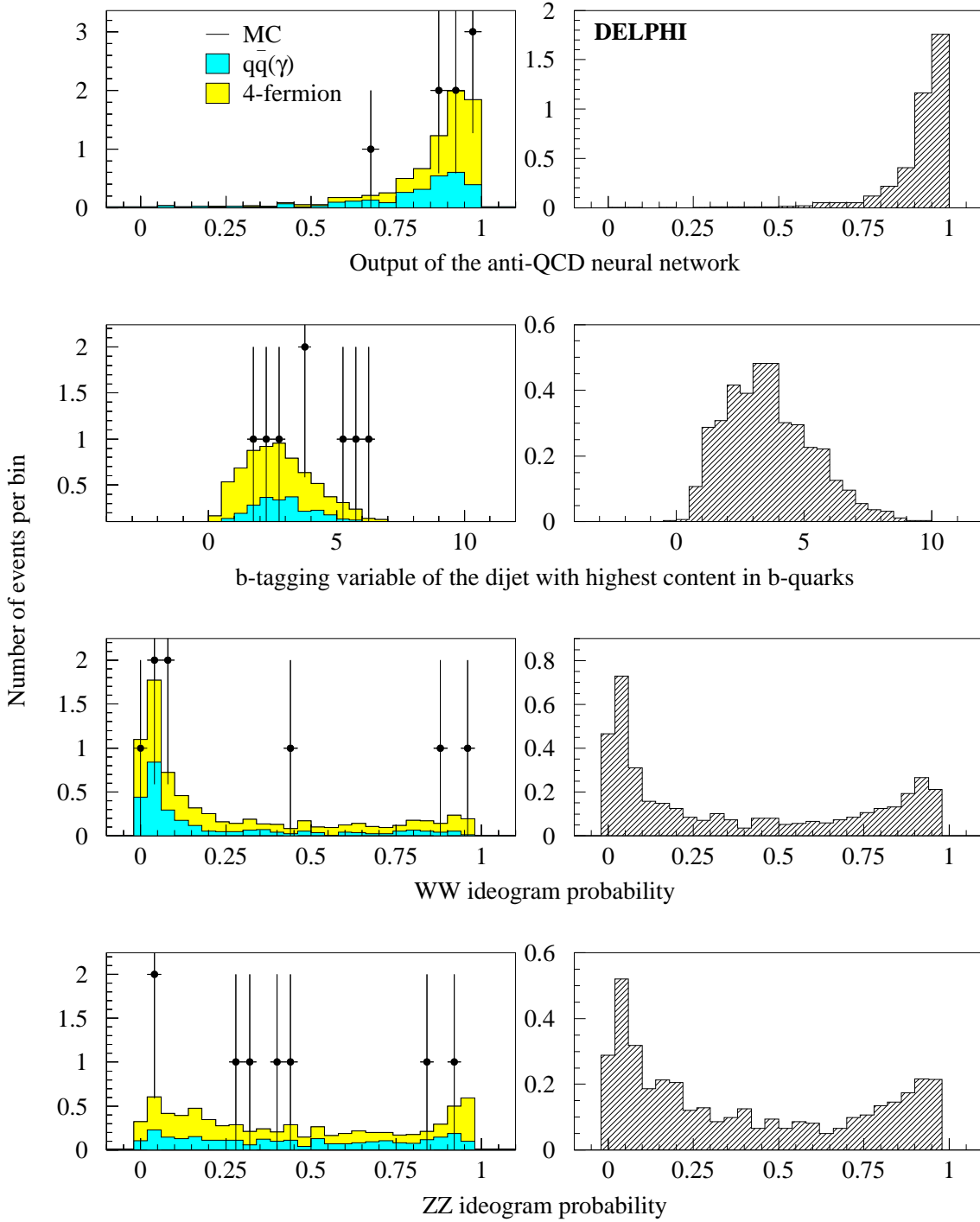


Figure 6: $Hq\bar{q}$ channel: same distribution as in Fig.5 but at the tight selection level.

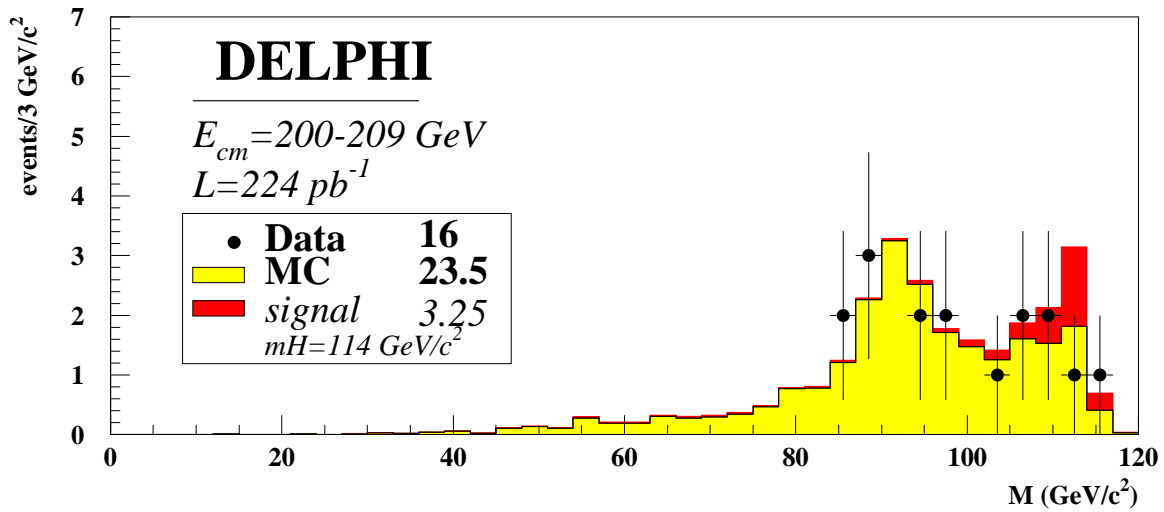


Figure 7: Distribution of the reconstructed mass of the candidates when combining all HZ analyses at 200-209 GeV in the year 2000. Data (dots) are compared with the Standard Model background expectations (light shaded histogram) and with the normalised 114 GeV/c² signal spectrum added to the background contributions (dark shaded histogram).

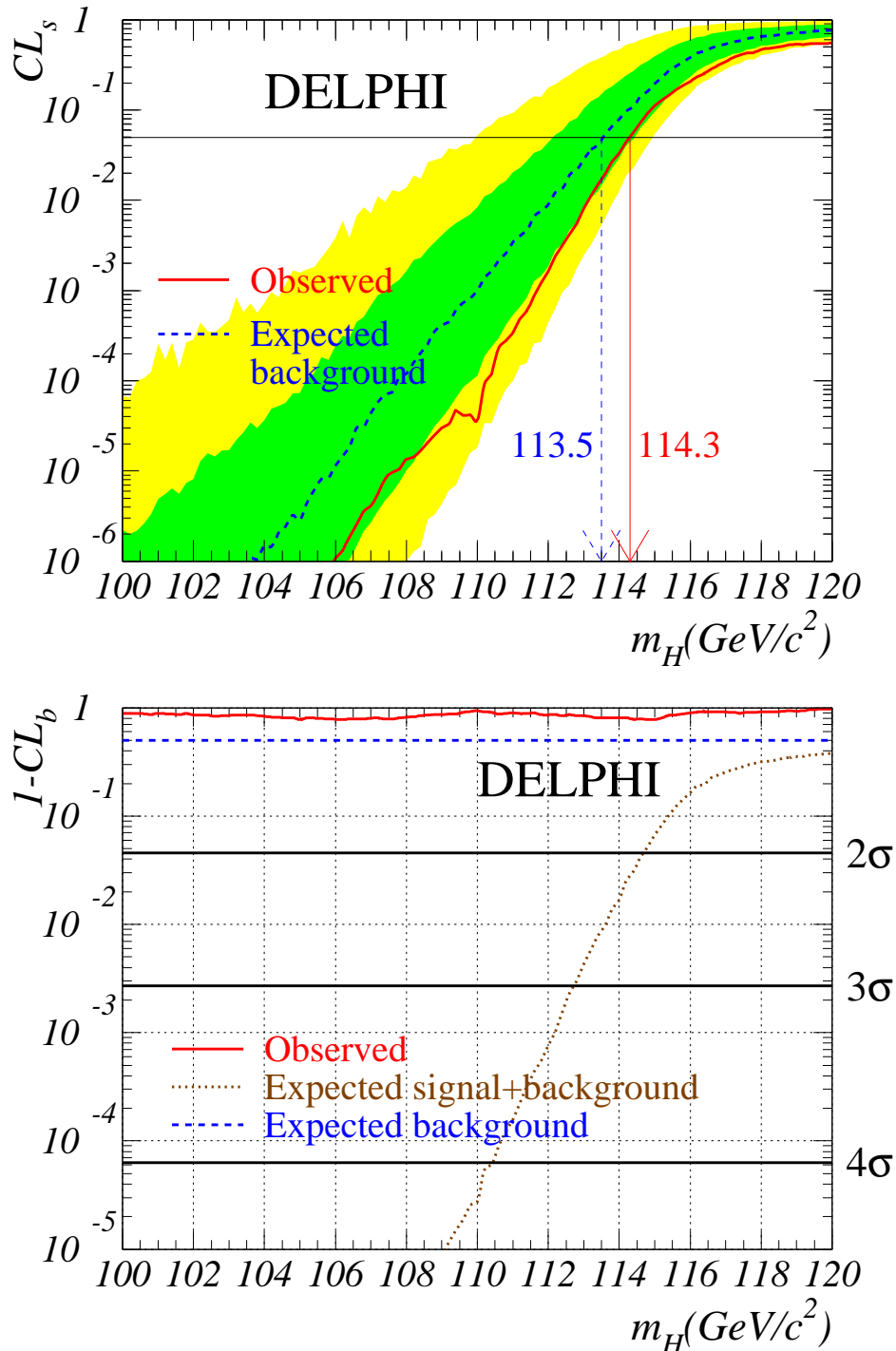


Figure 8: Confidence levels as a function of m_H . Curves are the observed (solid) and expected median (dashed) confidences from background-only experiments while the bands correspond to the 68% and 95% confidence intervals from background-only experiments. Top: CL_s , the confidence level for the signal hypothesis as a function of m_H . The intersections of the curves with the horizontal line at 5% define the observed and expected 95% CL lower limits on m_H at 114.3 and 113.5 GeV/c^2 respectively. Bottom: $1-CL_b$ for the background hypothesis. Also shown here is the curve of the median confidence as expected for a signal of mass given in abscissa (dotted line).

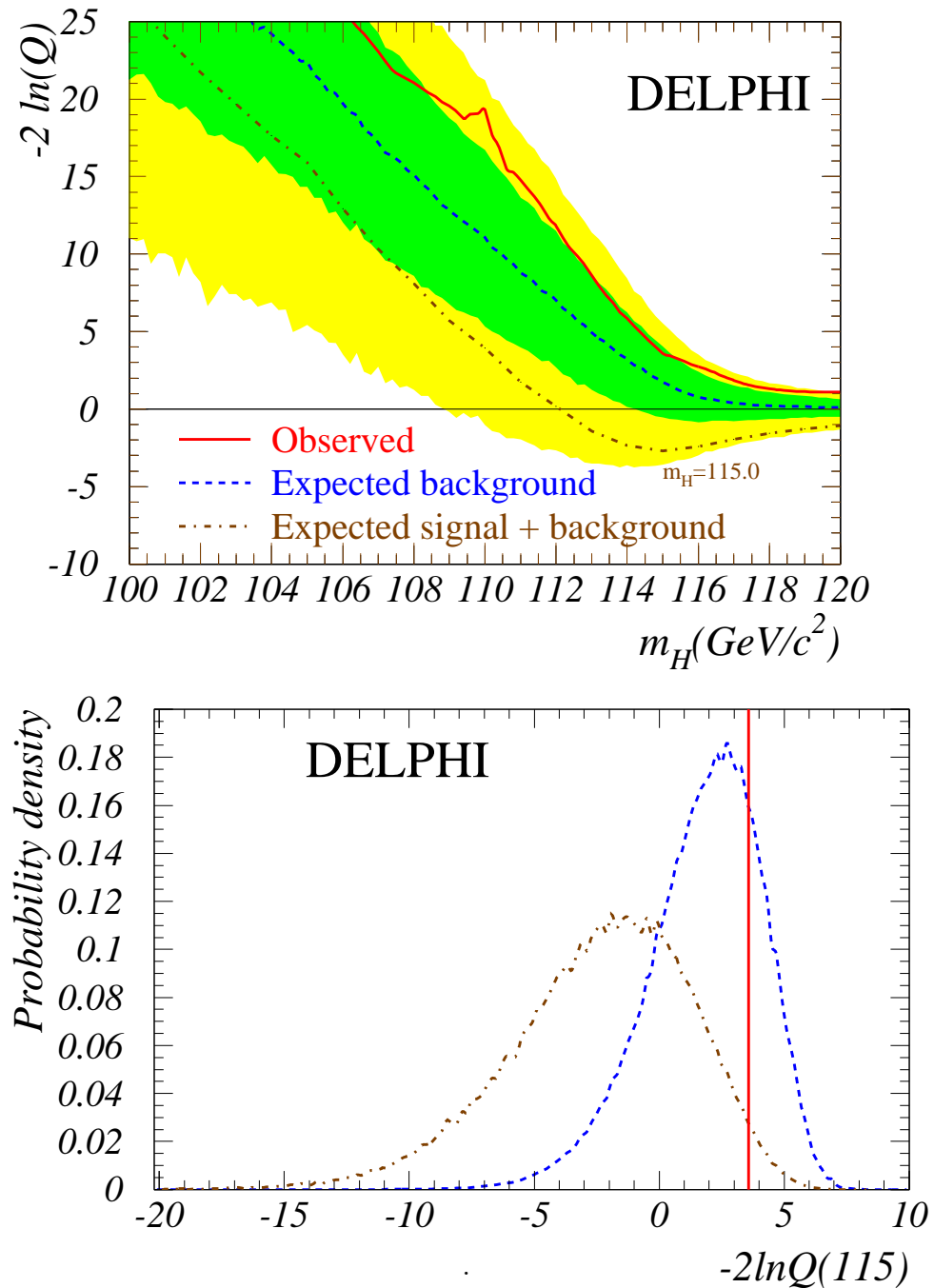


Figure 9: Top: the test-statistic (negative log-likelihood ratio) as a function of m_H . The observed value, full line, is compared to the expectation for the background only hypothesis, represented by the dashed line and the symmetric 68% and 95% probability shaded bands. The dot-dashed line shows the average expected result for a hypothetical Higgs mass of $115 \text{ GeV}/c^2$. Bottom: vertical slice of the previous plot for a mass value of $115 \text{ GeV}/c^2$, showing the sensitivity of the DELPHI result to this hypothesis. The dot-dashed line shows the expected distribution for signal plus background, the dashed line that for background only. The vertical line represents the data. The fractional area below the dashed curve and to the right of the data is CL_b ; for the dot-dashed curve it is $\text{CL}_{(s+b)}$.